Mercury anomalies associated with three extinction events (Capitanian Crisis, Latest Permian Extinction and the Smithian/Spathian Extinction) in NW Pangea

STEPHEN E. GRASBY*†‡, BENOIT BEAUCHAMP‡, DAVID P.G. BOND§,
PAUL B. WIGNALL¶ & HAMED SANEI*‡

*Geological Survey of Canada, 3303 33rd St N.W. Calgary AB Canada, T2L 2A7
‡Department of Geoscience, University of Calgary, Calgary AB Canada
§Department of Geography, Environment and Earth Sciences, University of Hull, Hull HU6 7RX, United Kingdom
¶School of Earth Sciences, University of Leeds, Woodhouse Lane, Leeds LS2 9JT, United Kingdom

Abstract – Strata of Permian – Early Triassic age that include a record of three major extinction events (Capitanian Crisis, Latest Permian Extinction and the Smithian/Spathian Extinction) were examined at the Festningen section, Spitsbergen. Over the *c.* 12 Ma record examined, mercury in the sediments shows relatively constant background values of 0.005–0.010 $\mu g\ g^{-1}$. However, there are notable spikes in Hg concentration over an order of magnitude above background associated with the three extinctions. The Hg/total organic carbon (TOC) ratio shows similar large spikes, indicating that they represent a true increase in Hg loading to the environment. We argue that these represent Hg loading events associated with enhanced Hg emissions from large igneous province (LIP) events that are synchronous with the extinctions. The Hg anomalies are consistent across the NW margin of Pangea, indicating that widespread mercury loading occurred. While this provides utility as a chemostratigraphic marker the Hg spikes may also indicate loading of toxic metals to the environment, a contributing cause to the mass extinction events.

Keywords: mercury, Early Triassic, Latest Permian Extinction, chemostratigraphy.

1. Introduction

Mercury (Hg) emissions associated with the emplacement of Large Igneous Provinces (LIPs) were first recognized by Sanei, Grasby & Beauchamp (2012), who showed a large Hg spike associated with the Siberian Traps eruptions. This event was coincident with the Latest Permian Extinction (LPE), the largest extinction in Earth's history that had a devastating impact on both terrestrial and marine ecosystems (Erwin, 2006). High Hg loading associated with the Siberian Traps has been supported by a similar Hg spike at the LPE boundary in Spitsbergen (Grasby *et al.* 2015). Recurrent Siberian Trap volcanism may also have influenced Hg loading during the Smithian/Spathian Extinction in the Sverdrup Basin (Grasby *et al.* 2013*b*). While these initial studies are focused on the sedimentary records from NW Pangea, the global extent of Hg loading related to Siberian Trap volcanism has yet to be demonstrated. However, subsequent work has shown similar Hg anomalies associated with other LIP events such as the Cretaceous–Palaeogene transition (Sial *et al.* 2013, 2014; Silva *et al.* 2013) related to Deccan Trap volcanism.

Hg is extremely toxic to life. This toxicity, combined with the ease of transport over long distances and

†Author for correspondence: sgrasby@nrcan.gc.ca

persistence of Hg in the environment, makes modern anthropogenic mercury emissions the subject of significant global concern (AMAP, 2011). The two largest natural source of Hg to the environment are volcanic emissions and natural coal combustion (Pirrone *et al.* 2010). These sources release Hg to the atmosphere where it can be globally transported prior to deposition in terrestrial and marine environments. In the marine environment, organic matter and clay minerals scavenge Hg and transport it to the sea floor to become fixed in bottom sediments (Cranston & Buckley, 1972; Andren & Harriss, 1975; Lindberg, Andrenson & Harrisson, 1975; Turner, Millward & Le Roux, 2004; Gehrke, Blum & Meyers, 2009). The control of primary productivity on Hg sequestration is shown by the close relationship between sedimentary organic matter and Hg in modern (Outridge *et al.* 2007; Stern *et al.* 2009; Sanei *et al.* 2014) as well as ancient sediments (Grasby *et al.* 2013*b*).

Modern volcanic eruptions have a significant Hg flux that produces global Hg anomalies (Slemr *et al.* 1995; Slemr & Scheel, 1998; Schuster *et al.* 2002; Pyle & Mather, 2003). Hg is sourced from both volcanic gases as well as from rock units intruded by magma (Sanei, Grasby & Beauchamp, 2012, 2015; Grasby *et al.* 2015). During LIP events emission rates would greatly exceed normal Hg release (Sanei, Grasby & Beauchamp, 2012; Grasby *et al.* 2015), such that the normal

Figure 1. Map showing location of the Festningen section on Spitsbergen (base of section is located at 78.0950° N, 13.8240° E (WGS84 datum).

marine buffering control on Hg can be potentially overwhelmed (Sanei, Grasby & Beauchamp, 2012; Grasby *et al.* 2013*b*) and be recorded as an Hg spike in the sediment record. For instance, Grasby *et al.* (2015) estimated that the Siberian Traps may have released up to 9.98 Gg a^{-1} Hg, or 400 % above modern natural emissions. In comparision, the modern anthropogenic Hg emissions that roughly equal natural emissions are the subject of global concern over their impact on marine and terrestrial ecosystems. Hg anomalies formed at the time of LIP eruptions therefore suggest that: (1) Hg could be an effective marker in the geological record of periods of enhanced volcanic activity; and (2) LIP eruptions could potentially release toxic amounts of Hg to the environment. Such a scenario would add to the variety of kill mechanisms already associated with major volcanic eruptions (Keller & Kerr, 2014), as well as providing a direct link between terrestrial and marine extinction.

To further the assessment of Hg in the geological record, we examined the Permian – Early Triassic record at the Festningen section in Spitsbergen (Fig. 1). This well-known location records the LPE (Grasby *et al.* 2015; Wignall, Morante & Newton, 1998) as well as evidence for the earlier Capitanian Crisis (Bond *et al.* 2015) and Smithian/Spathian Extinction (Wignall *et al.* this volume), all of which have been linked to periods of major volcanic activity. Of these recent studies, the Hg record at Festningen has only been examined in a nar-

row (40 m) zone straddling the LPE boundary (Grasby *et al.* 2015). In this paper we examine the Hg record at Festningen over 600 m of section, spanning middle Permian – Lower Triassic deposits, representing *c.* 12 million years of Earth's history.4.

2. Study area

The Festningen section is located at Kapp Starostin, Spitsbergen (Fig. 1). The *c.* 45° east-dipping beds occur along a low-elevation sea cliff of *c.* 7 km in length. The section provides a near-continuous exposure of Carboniferous–Cenozoic strata, from Kapp Starostin to Festningsdodden, deposited in a distal broad epicontinental shelf setting on the north-western margin of Pangea (Wignall, Morante & Newton, 1998; Stemmerik & Worsley, 2005; Blomeier *et al.* 2013). During Permian time Spitsbergen was at a palaeolatitude of *c.* 40–45° N (Golonka & Ford, 2000; Scotese, 2004).

The Kapp Starostin Formation was deposited during a period of passive subsidence that followed a major relative sea-level drop at the lower–middle Permian boundary (Blomeier *et al.* 2013). Deposition of widespread heterozoan carbonate (Vøringen Member) occurred during Roadian time, followed by the progradation of heterozoan carbonates and cherts over much of the Barents Shelf and Svalbard (Blomeier *et al.* 2013). Spitsbergen shares a similar depositional history to the palaeogeographically adjoining Sverdrup
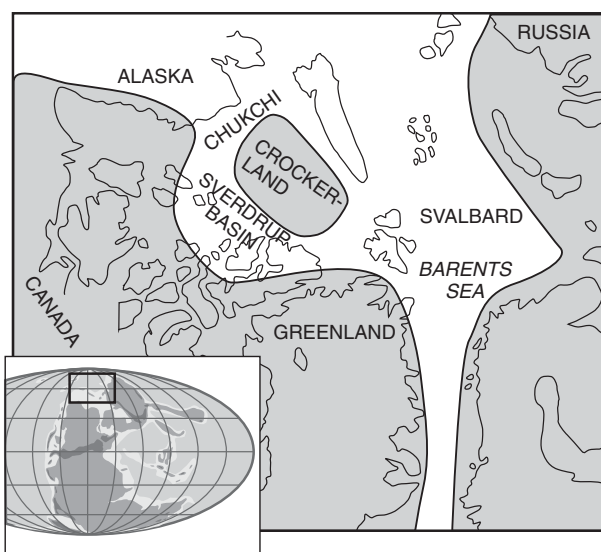
Figure 2. Palaeogeographic map (after Embry, 1992) showing relative location of Sverdrup Basin and Spitsbergen. Inset map (after Scotese, 2004) showing location on NW Pangea.

Basin (van Hauen, Degerböls and Trold Fiord formations; Beauchamp *et al.* 2009; Fig. 2). Approximately 40 m below the contact with the overlying uppermost Permian – Lower Triassic Vardebukta Formation, fossiliferous carbonates of the Kapp Starostin Formation transition to spiculitic chert of late Permian age (Blomeier *et al.* 2013). These later Permian chert beds are considered equivalent to the Black Stripe and Lindström formations of the Sverdrup Basin (Beauchamp *et al.* 2009). The Vardebukta and overlying Tvillingodden formations are dominated by shale, siltstone and minor sandstone of Early–Middle Triassic age (Mørk, Knarud & Worsley, 1982), equivalent to the Blind Fiord Formation of the Sverdrup Basin (Embry, 1989). The basal *c.* 6–7 m of the Vardebukta Formation is latest Permian in age (Wignall, Morante & Newton, 1998; Grasby *et al.* 2015).

3. Methods

A detailed sample suite was collected from 100 m below the Kapp Starostin/Vardebukta contact to 500 m above. Sample spacing varied from 1–2 m away from the contact to a higher density of 20–50 cm spacing from *c.* 40 m below to 19 m above the top of the Kapp Starostin Formation. Samples were recorded in metres above (positive) and below (negative) the last chert bed that defines the top of the Kapp Starostin Formation. Weathered surfaces were removed and then samples were collected from an isolated layer no greater than 2 cm thick. In the laboratory, any remaining weathered surfaces were removed and fresh samples were powdered by agate mortar and pestle.

Total organic carbon (TOC) was measured using Rock-Eval 6$^{\copyright}$, with $\pm 5\%$ analytical error of reported value, based on repeats and reproducibility

of standards run after every fifth sample (Lafargue *et al.* 1998). Elemental determinations were conducted on powdered samples digested in a 2:2:1:1 acid solution of H_2O–HF–$HClO_4$–HNO_3, and subsequently analysed using a PerkinElmer Elan 9000 mass spectrometer with $\pm 2\%$ analytical error. Hg was measured at GSC-Atlantic by LECO$^{\circledR}$ AMA254 mercury analyser (Hall & Pelchat, 1997) ($\pm 10\%$). $\delta^{13}C_{org}$ was determined on samples washed with hydrochloric acid, and rinsed with hot distilled water to remove any carbonate. $\delta^{13}C$ was measured using continuous-flow elemental-analysis isotope-ratio mass spectrometry, with a Finnigan Mat Delta+XL mass spectrometer interfaced with a Costech 4010 elemental analyser with combined analytical and sampling error of $\pm 0.2\,‰$.

Analytical results from a total of 341 samples used in this study are provided in Table 1.

4. Results

4.a. Organic carbon

The organic carbon record, expressed as percent TOC, shows low values ($<1\%$ TOC) overall (Fig. 3a). There is an increase in TOC at –40 m. Based on brachiopod, Sr isotopes records and magnetostratigraphy data, Bond *et al.* (2015) argue that the –40 m level is around the middle Permian extinction level at Festningen. The TOC values decline again leading up to the LPE boundary, where there is a second brief increase in TOC just above the LPE. For the remainder of the section, TOC values in the Vardebukta Formation are $<0.2\%$. At these low values the accuracy of Rock-Eval results decreases, however data are plotted in Figure 3a to illustrate the overall low TOC values through this interval. The TOC values increase again in the basal Tvillingodden Formation, before dropping to low values in the upper 100 m of section.

Rock-Eval 6$^{\copyright}$ results also provided information on thermal maturation and indicated that organic matter in the shales have never been heated past the upper end of the oil window, and consequently the stable isotope values of organic carbon were not thermally altered (Hayes, Kaplan & Wedeking, 1983). The only exception is a local thermal anomaly associated with a sill emplaced at *c.* 19 m that does not extend beyond 5 m of the sill boundary (Grasby *et al.* 2015).

4.b. Carbon isotope record

Portions of the organic carbon isotope curve ($\delta^{13}C_{org}$) at the Festningen section have been reported in previous studies, including middle–upper Permian sediments (Bond *et al.* 2015), across the Latest Permian Extinction event (Grasby *et al.* 2015) and sediments of Early Triassic age (Wignall *et al.* this volume). The combined $\delta^{13}C_{org}$ curve is provided here (Fig. 3b) for comparison with both organic carbon isotope data from NW Pangea and the global inorganic carbon

Table 1. Geochemical data from the Festningen section. Depths are measured relative to the Latest Permian Extinction (LPE) Boundary marked by the top of the Kapp Starostin Formation. ND – not determined.

Sample ID	Depth relative to LPE (m)	$\delta^{13}C$ org (‰)	Hg (ppb)	TOC (%)	Mo (ppm)	Al (%)
C-556979	− 97.7	− 24.5	9	0.02	0.45	0.54
C-556980	− 97.2	− 21.0	5	0.07	0.48	0.31
C-556981	− 95.7	− 22.2	4	0.05	0	0.59
C-556982	− 94.2	ND	5	0.04	0	0.58
C-556983	− 92.7	− 22.4	6	0.11	0.09	1.02
C-556984	− 91.2	− 23.0	2	0.01	0.05	0.42
C-556985	− 89.7	− 23.0	2	0.02	0.07	0.3
C-556986	− 86.7	− 25.0	11	0.22	0.31	1.59
C-556987	− 83.7	− 24.0	7	0.11	0.2	1.15
C-556988	− 80.7	− 23.7	5	0.02	0.08	0.6
C-556989	− 77.7	− 25.0	6	0.03	0.22	0.61
C-556990	− 74.7	− 23.8	9	0.12	0.1	1.55
C-556991	− 71.7	− 24.3	6	0.02	0	0.53
C-556992	− 68.7	− 24.5	4	0.02	0	0.71
C-556993	− 65.7	− 25.5	4	0.05	0	0.64
C-556994	− 62.7	− 24.4	4	0.01	0	0.85
C-556995	− 59.7	− 24.8	4	0.03	0.08	0.59
C-556996	− 56.7	− 24.6	4	0.07	0.09	0.75
C-556997	− 53.7	− 25.2	4	0.07	0.21	1.21
C-556998	− 50.7	− 25.3	3	0.10	0	1.01
C-556999	− 47.7	− 24.5	4	0.01	0	0.7
C-557000	− 46.2	− 24.9	9	0.09	0.13	1
C-557001	− 44.7	− 24.5	6	0.05	0.13	1.28
C-557002	− 43.2	− 24.2	5	0.03	0.08	0.9
C-557003	− 41.7	− 23.6	6	0.08	0.06	0.45
C-557004	− 40.2	− 23.3	7	0.04	0.2	1.55
C-556572	− 27.2	− 24.3	28	0.25	0.53	2.65
C-556573	− 26.7	− 24.6	34	0.44	0.82	4.18
C-556574	− 26.2	− 24.6	36	0.39	0.99	3.85
C-556575	− 25.7	− 24.4	22	0.33	0.57	3.63
C-556576	− 25.2	− 24.7	22	0.29	2.66	2.84
C-556577	− 24.7	− 24.5	17	0.22	1.05	2.6
C-556578	− 24.2	− 24.4	35	0.34	1.83	3.3
C-556579	− 23.7	− 24.0	41	0.43	0	
C-556580	− 23.2	− 23.8	34	0.49	0.34	3.68
C-556581	− 22.2	− 23.74	48	0.65	0.25	4.36
C-556582	− 21.7	− 23.6	42	0.69	0.39	4.43
C-556583	− 21.2	− 23.63	38	0.59	0.26	4.21
C-556584	− 20.7	− 23.87	30	0.60	0.48	4.26
C-556585	− 20.2	− 23.62	37	0.58	0.46	4.54
C-556586	− 19.7	− 23.6	33	0.55	0.46	4.67
C-556587	− 18.2	− 23.86	28	0.51	0.8	4.19
C-556588	− 17.7	− 23.88	30	0.50	0.97	4.18
C-556589	− 17.2	− 23.9	33	0.57	1.26	3.97
C-556590	− 16.7	− 23.7	28	0.45	0.52	3.69
C-556591	− 16.2	− 24.0	29	0.49	0.7	4.2
C-556592	− 15.7	− 23.3	31	0.45	0.66	4.62
C-556593	− 15.2	− 24.0	30	0.53	0.74	4.08
C-556594	− 14.7	− 23.6	30	0.41	0.34	4.35
C-556595	− 14.2	− 24.1	32	0.44	0.33	4.07
C-556596	− 13.7	− 23.9	38	0.65	0.22	5.28
C-556597	− 13.2	− 23.7	34	0.50	0.31	4.7
C-556598	− 12.7	− 24.0	33	0.48	0.63	4.7
C-556599	− 12.2	− 24.3	37	0.56	0.57	5.4
C-556600	− 11.7	− 24.2	38	0.64	0.59	5.58
C-556601	− 11.2	− 25.2	14	0.44	0.44	3.85
C-556602	− 10.7	− 25.1	13	0.36	0.69	4.19
C-556603	− 10.2	− 24.9	13	0.35	1.13	3.6
C-556604	− 9.7	− 24.9	13	0.21	0.73	2.5
C-556605	− 9.2	− 25.5	17	0.35	0.83	4.2
C-556606	− 8.7	− 25.4	14	0.45	1.01	3.92
C-556607	− 8.2	− 24.7	16	0.35	0.68	3.69
C-556608	− 7.7	− 25.6	13	0.32	0.73	3
C-556609	− 7.2	− 25.0	15	0.37	0.48	3.32
C-556610	− 6.7	− 24.6	16	0.37	0.63	3.2
C-556611	− 6.2	− 24.5	13	0.40	0.48	3.42
C-556612	− 5.7	− 24.3	13	0.29	0.29	3.37
C-556613	− 5.2	− 24.3	16	0.29	0.45	3.11
C-556614	− 4.7	− 24.7	9	0.45	0.38	4
C-556615	− 4.2	− 25.2	14	0.52	0.76	3.22
C-556616	− 3.7	− 25.2	14	0.24	0.79	2.89
C-556617	− 3.2	− 25.7	17	0.24	0.84	2.67
C-556618	− 3	− 25.5	16	0.22	0.72	2.77

Table 1. Continued.

Sample ID	Depth relative to LPE (m)	δ^{13}C org (‰)	Hg (ppb)	TOC (%)	Mo (ppm)	Al (%)
C-556619	− 3.45	− 25.1	15	0.19	2.92	1.66
C-556620	− 2.8	− 25.3	22	0.40	0.62	4.48
C-556621	− 2.6	− 25.7	19	0.39	0.82	4.04
C-556622	− 2.4	− 25.9	18	0.33	0.96	3.84
C-556623	− 2.2	− 26.1	24	0.39	0.92	3.83
C-556624	− 2	− 25.6	19	0.41	0.6	3.84
C-556625	− 1.8	− 25.7	15	0.34	0.8	3.57
C-556626	− 1.6	− 25.6	17	0.46	0.89	3.9
C-556627	− 1.4	− 24.8	18	0.35	0.36	4.17
C-556628	− 1.2	− 25.6	24	0.30	1.14	3.65
C-556629	− 1	− 25.5	15	0.22	1.31	3.5
C-556630	− 0.8	− 25.1	18	0.30	0.75	3.82
C-556631	− 0.6	− 24.5	20	0.29	0.41	3.43
C-556632	− 0.4	− 24.2	21	0.39	0.77	4.33
C-556633	− 0.2	− 25.3	16	0.23	0.57	3.42
C-556634	0	− 25.5	20	0.33	1.37	3.33
C-556635	1	− 29.0	29	0.28	0.48	7.98
C-556636	1.2	− 29.6	43	0.24	1.07	8.21
C-556637	1.4	− 29.1	48	0.19	1.34	8.69
C-556638	1.6	− 28.8	33	0.13	1.21	8.45
C-556639	1.8	− 28.6	27	0.14	0.28	8.25
C-556640	2	− 28.7	26	0.11	0.52	8.52
C-556641	2.2	− 28.8	16	0.10	0.14	8.57
C-556642	2.4	− 28.9	20	0.09	0.16	8.57
C-556643	2.6	− 30.1	30	0.13	0.46	9.98
C-556644	2.8	− 30.4	17	0.10	0.14	7.85
C-556645	2.9	− 30.3	25	0.08	0.46	9.5
C-556646	3.1	− 30.8	25	0.12	0.17	7.87
C-556647	3.3	− 31.0	27	0.22	0.16	8.2
C-556648	3.5	− 32.8	41	0.40	0.55	7.96
C-556649	3.7	− 32.6	43	0.45	0.96	8.09
C-556650	3.9	− 32.5	42	0.43	0.57	8.21
C-556651	4.1	− 33.5	77	0.31	4.4	9.75
C-556652	4.3	− 32.8	60	0.48	1.59	7.87
C-556653	4.4	− 32.6	74	0.27	0.63	8.05
C-556654	5.4	− 32.5	62	0.50	1.43	7.99
C-556655	5.6	− 32.2	53	0.33	1.23	8.19
C-556656	5.8	− 33.3	86	0.42	2.39	9.91
C-556657	6	− 32.6	69	0.44	0.76	9.66
C-556658	6.2	− 33.2	69	0.31	0.57	9.77
C-556659	6.4	− 33.6	60	0.39	1.04	8.47
C-556660	6.6	− 33.3	53	0.28	0.48	10.3
C-556661	6.8	− 33.2	46	0.26	0.35	10.97
C-556662	7	− 32.8	53	0.34	0.44	11.28
C-556663	7.2	− 32.6	51	0.34	0.52	10.92
C-556664	7.4	− 33.0	50	0.31	0.39	10.76
C-556665	7.6	− 32.9	81	0.44	2.76	10.02
C-556666	7.8	− 32.9	77	0.56	5.03	8.99
C-556667	8	− 32.3	82	0.71	3.91	9.56
C-556668	8.15	− 32.7	89	0.51	5.2	7.92
C-556669	8.2	− 33.7	134	1.03	20.65	8.74
C-556670	8.4	− 33.0	88	0.63	10.16	7.12
C-556671	8.6	− 33.5	100	0.61	26.37	7.02
C-556672	8.8	− 33.6	57	0.38	4.51	9.62
C-556673	9	− 33.8	57	0.41	3.67	9.2
C-556674	9.2	− 32.1	25	0.08	1.58	6.99
C-556675	9.4	− 33.3	50	0.46	2.77	9.55
C-556676	9.6	− 32.8	38	0.25	0.59	10.06
C-556677	9.8	− 33.1	26	0.30	0.96	9.54
C-556678	10	− 32.9	47	0.23	0.62	10.87
C-556679	10.2	− 33.2	35	0.30	1.02	10.63
C-556680	10.4	− 33.0	30	0.29	1.92	10.99
C-556681	10.6	− 32.8	40	0.49	1.98	9.53
C-556682	10.8	− 31.6	19	0.14	1.42	6.76
C-556683	11	− 31.8	23	0.17	1.4	9.02
C-556684	11.2	− 27.4	74	1.02	1.41	9.1
C-556685	11.4	− 31.8	34	0.17	2.14	8.21
C-556686	11.6	− 32.1	23	0.21	0.83	9.45
C-556687	11.8	− 32.2	31	0.25	1.51	9.31
C-556688	12	− 32.6	48	0.39	3.08	9.09
C-556689	12.2	− 32.6	56	0.55	2.9	9.23
C-556690	12.4	− 31.3	19	0.09	1.28	6.7
C-556691	12.6	− 33.1	34	0.29	2.55	9.55
C-556692	12.8	− 32.7	35	0.15	3.04	6.67

Table 1. Continued.

Sample ID	Depth relative to LPE (m)	δ¹³C org (‰)	Hg (ppb)	TOC (%)	Mo (ppm)	Al (%)
C-556693	13	− 33.1	45	0.33	7.18	7.38
C-556694	13.2	− 32.8	47	0.29	4	7.1
C-556695	13.05	− 33.9	41	0.48	12.34	9.75
C-556696	13.4	− 32.7	34	0.30	4.13	7.19
C-556697	13.6	− 33.6	42	0.50	4.96	7.1
C-556698	13.8	− 33.3	43	0.48	3.89	7.31
C-556699	14	− 32.4	35	0.17	2.55	7.44
C-556700	14.2	− 33.4	27	0.31	3.45	4.54
C-556701	14.4	− 33.5	24	0.26	3.5	4.57
C-556702	14.8	− 32.8	33	0.45	2.31	7.7
C-556703	15.3	− 32.4	15	0.18	1.71	7.25
C-556704	15.8	− 31.2	10	0.10	0.37	7.99
C-556705	16.3	− 31.8	7	0.28	1.53	7.82
C-556706	16.8	− 32.4	1	0.35	1.27	7.98
C-556707	17.3	− 32.4	1	0.19	3.08	8.2
C-556708	17.8	− 25.1	0.43	0.00	3.34	7.79
C-556709	18.8	ND	0.49	0.01	3.01	7.72
C-556710	20.3	− 31.9	0.36	0.19	3.51	7.98
C-556711	21.8	− 32.6	4	0.16	1.32	8.08
C-556712	23.3	− 32.5	18	0.64	3.42	7.49
C-556713	24.8	− 33.0	20	0.42	2.66	7.43
C-556714	26.3	− 32.7	22	0.50	2.96	7.07
C-556715	27.8	− 32.7	26	0.54	2.9	7.03
C-556716	29.3	− 32.8	25	0.40	1.21	7.42
C-556717	30.8	− 32.3	24	0.32	1.36	7.1
C-556718	32.3	− 32.8	31	0.73	3.33	7.09
C-556719	33.8	− 32.1	34	0.57	2.31	7.16
C-556720	35.3	− 31.3	23	0.35	1.04	7.42
C-556721	36.8	− 31.8	18	0.49	3.17	7.3
C-556722	38.3	− 31.7	9	0.23	0.4	6.65
C-556723	39.8	− 31.3	9	0.26	0.8	7.43
C-556724	41.3	− 31.3	16	0.30	0.42	7.29
C-556725	44.3	− 31.5	22	0.49	0.75	7.38
C-556726	47.3	− 31.4	29	0.62	0.71	6.84
C-556727	50.3	− 31.1	27	0.45	0.36	7.16
C-556728	53.3	− 29.2	9	0.05	0.55	4.44
C-556729	56.3	− 29.9	16	0.12	0.42	6.64
C-556730	59.3	− 29.7	11	0.15	0.33	6.94
C-556731	62.3	− 28.7	10	0.15	0.17	7.56
C-556732	65.3	− 29.2	8	0.12	0.29	6.92
C-556733	68.3	− 29.8	5	0.07	0.28	6.51
C-556734	71.3	− 29.6	8	0.09	0.59	6.67
C-556735	74.3	− 29.6	8	0.10	0.46	6.01
C-556736	77.3	− 29.5	5	0.06	0.31	6.88
C-556737	80.3	− 29.4	7	0.07	0.29	6.66
C-556738	83.3	− 29.2	7	0.06	0.26	6.43
C-556739	86.3	− 28.6	4	0.04	0.27	6.58
C-556740	89.3	− 29.1	14	0.11	0.64	6.84
C-556741	92.3	− 28.5	5	0.05	0.19	6.32
C-556742	95.3	− 27.9	8	0.13	0.23	6.24
C-556743	98.3	− 28.5	5	0.05	0.28	6.36
C-556744	101.3	− 28.0	4	0.11	0.24	5.53
C-556745	104.3	− 28.3	8	0.05	0.25	5.57
C-556746	107.3	− 27.6	3	0.03	0.16	6.66
C-556747	110.3	− 28.3	5	0.12	0.25	6.04
C-556748	113.3	− 27.6	4	0.02	0.18	5.84
C-556749	116.3	− 27.8	12	0.03	0.45	4.94
C-556750	117.8	− 28.7	16	0.15	0.85	6.42
C-556751	119.3	− 28.3	22	0.16	0.45	6.54
C-556752	122.3	− 28.9	16	0.07	0.51	4.1
C-556753	125.3	− 27.6	14	0.06	0.3	5.12
C-556754	128.3	− 26.7	9	0.04	0.3	5.95
C-556755	134.3	− 27.4	10	0.06	0.22	6.44
C-556756	137.3	− 27.7	4	0.02	0.16	6.36
C-556757	140.3	− 26.8	8	0.04	0.27	6.19
C-556758	143.3	− 28.3	30	0.28	0.82	6.06
C-556759	146.3	− 27.2	21	0.09	0.27	5.97
C-556760	149.3	− 26.7	10	0.08	0.29	6.92
C-556761	152.3	− 26.7	16	0.10	0.19	6.55
C-556762	153.3	− 26.0	7	0.03	0.25	6.03
C-556763	154.8	− 26.0	22	0.11	0.38	6.86
C-556764	157.8	− 26.9	10	0.07	0.18	6.32
C-556765	160.8	− 27.4	17	0.12	0.27	7.81
C-556766	163.8	− 26.8	7	0.02	0.41	6.26

Table 1. Continued.

Sample ID	Depth relative to LPE (m)	$\delta^{13}C$ org (‰)	Hg (ppb)	TOC (%)	Mo (ppm)	Al (%)
C-556767	166.8	− 26.3	9	0.11	0.29	6.92
C-556768	169.8	− 26.1	9	0.05	0.22	6.75
C-556769	182.3	− 26.5	4	0.04	0.19	5.03
C-556770	196.8	− 24.7	7	0.06	0.18	5.23
C-556771	199.8	− 25.7	7	0.03	0.14	6.66
C-556772	202.8	− 25.7	4	0.02	0.13	6.27
C-556773	205.8	− 26.0	4	0.01	0.18	4.37
C-556774	208.8	− 26.1	5	0.07	0.16	5.78
C-556775	214.8	− 26.0	3	0.01	0.08	5.68
C-556776	217.8	− 26.6	5	0.02	0.14	6.88
C-556777	220.8	− 27.1	7	0.04	0.11	6.86
C-556778	223.8	− 27.4	5	0.02	0.15	6.06
C-556779	226.8	− 26.8	5	0.09	0.16	5.99
C-556780	229.8	− 27.1	7	0.02	0.18	5.1
C-556781	232.8	− 28.7	10	0.05	0.14	5.21
C-556782	235.8	− 27.4	10	0.03	0.41	4.33
C-556783	238.8	− 27.4	6	0.03	0.18	6.22
C-556784	241.8	− 27.7	8	0.06	0.24	6.65
C-556785	244.8	− 28.1	11	0.06	0.29	5.71
C-556786	247.8	− 29.2	8	0.06	0.2	5.61
C-556787	250.8	− 29.4	7	0.06	0.2	6.31
C-556788	253.8	− 28.5	5	0.05	0.19	5.81
C-556789	256.8	− 31.1	11	0.15	0.32	6.17
C-556790	260.8	− 29.7	12	0.09	0.31	6.36
C-556791	263.8	− 29.4	9	0.06	0.44	5.57
C-556792	266.8	− 31.4	14	0.13	0.3	6.08
C-556793	269.8	− 31.6	13	0.19	0.43	5.85
C-556794	272.8	− 31.5	15	0.16	0.39	6.14
C-556795	275.8	− 28.7	5	0.05	0.14	6.15
C-556796	278.8	− 30.2	6	0.10	0.15	5.37
C-556797	281.8	− 30.7	5	0.05	0.18	5.13
C-556798	284.8	− 31.4	12	0.11	0.62	5.93
C-556799	290.8	− 30.1	5	0.06	0.31	5.87
C-556800	293.8	− 31.2	15	0.15	1.08	6.6
C-556801	296.8	− 31.3	10	0.15	1.09	6.19
C-556802	299.8	− 32.5	54	0.50	7.52	6.65
C-556803	302.8	− 32.7	55	0.30	10.08	5.56
C-556804	309.8	− 32.4	43	0.32	5.94	5.81
C-556805	312.8	− 32.9	36	0.23	8.15	4.67
C-556806	315.8	− 32.8	65	0.48	11.74	6
C-556807	318.8	− 30.6	38	0.43	1.46	6.31
C-556808	321.8	− 30.7	32	0.46	1.77	5.93
C-556809	324.8	− 30.6	28	0.57	1.54	5.72
C-556810	327.8	− 29.9	16	0.28	0.57	5.41
C-556811	330.8	− 29.6	23	0.49	0.73	6.23
C-556812	333.8	− 30.3	30	0.46	1.55	6.23
C-556813	336.8	− 29.6	32	0.61	1.88	6.43
C-556814	339.8	− 29.3	11	0.20	0.48	5.07
C-556815	342.8	− 28.6	26	0.62	7.48	5.08
C-556816	345.8	− 28.7	26	0.91	8.42	6.32
C-556817	348.8	− 28.6	18	0.62	3.14	6.27
C-556818	351.8	− 28.6	8	0.22	1.44	4.98
C-556819	354.8	− 29.1	19	0.93	1.33	6.25
C-556820	357.8	− 29.4	19	0.95	0.99	5.79
C-556821	360.8	− 29.3	21	1.13	0.83	6.51
C-556822	363.8	− 29.1	14	0.66	0.52	6.06
C-556823	366.8	− 29.6	13	0.43	2.08	4.21
C-556824	369.8	− 30.2	26	0.86	4.3	6.68
C-556825	372.8	− 30.5	24	0.80	3.07	6.7
C-556826	375.8	− 30.6	19	0.43	2.47	5.69
C-556827	378.8	− 30.7	17	0.38	2.11	5.7
C-556828	381.8	− 30.5	15	0.25	2.61	5.96
C-556829	387.8	− 30.7	12	0.30	2.45	5.74
C-556830	390.8	− 30.6	13	0.28	0.8	5.75
C-556831	393.8	− 30.4	8	0.23	0.76	4.31
C-556832	396.8	− 30.6	10	0.28	0.44	4.86
C-556833	399.8	− 30.8	13	0.42	0.79	5.86
C-556834	402.8	− 30.5	11	0.34	0.54	5.84
C-556835	405.8	− 30.1	6	0.15	0.36	3.72
C-556836	408.8	− 30.8	8	0.25	1.1	4.54
C-556837	411.8	− 30.8	12	0.28	1.41	4.96
C-556838	414.8	− 31.5	20	0.53	3.72	6.7
C-556839	417.8	− 31.3	13	0.33	1.99	6
C-556840	420.8	− 30.9	13	0.21	1.96	5.37

Table 1. Continued.

Sample ID	Depth relative to LPE (m)	$\delta^{13}C$ org (‰)	Hg (ppb)	TOC (%)	Mo (ppm)	Al (%)
C-556841	423.8	−31.5	12	0.37	1.17	5.94
C-556842	426.8	−30.4	6	0.11	1.2	3.86
C-556843	429.8	−31.4	11	0.34	3.49	5.8
C-556844	432.8	−31.0	9	0.26	2.28	3.79
C-556845	435.8	−31.7	17	0.54	6.92	5.49
C-556846	438.8	−31.8	11	0.25	6.32	4.44
C-556847	441.8	−31.2	6	0.19	1.7	3.85
C-556848	444.8	−30.3	4	0.11	1.99	3.37
C-556849	447.8	−31.2	6	0.20	5.56	4.08
C-556850	450.8	−30.9	6	0.22	6.11	3.81
C-556851	453.8	−30.5	8	0.13	2.78	2.99
C-556852	456.8	−31.1	10	0.16	3.47	3.68
C-556853	459.8	−29.7	4	0.07	0.66	4.23
C-556854	462.8	−30.4	6	0.10	1.8	3.73
C-556855	468.3	−28.4	7	0.11	0.25	4.19
C-556856	475.3	−29.6	5	0.10	1.23	4.87
C-556857	479.8	−30.2	7	0.11	0.45	4.62
C-556858	482.8	−30.3	7	0.14	0.55	4.04
C-556859	485.8	−29.5	8	0.14	0.75	4.93
C-556860	488.8	−28.5	3	0.05	0.22	3.78
C-556861	491.8	−29.8	7	0.12	0.42	4.09
C-556862	499.8	−30.0	7	0.24	0.63	3.98
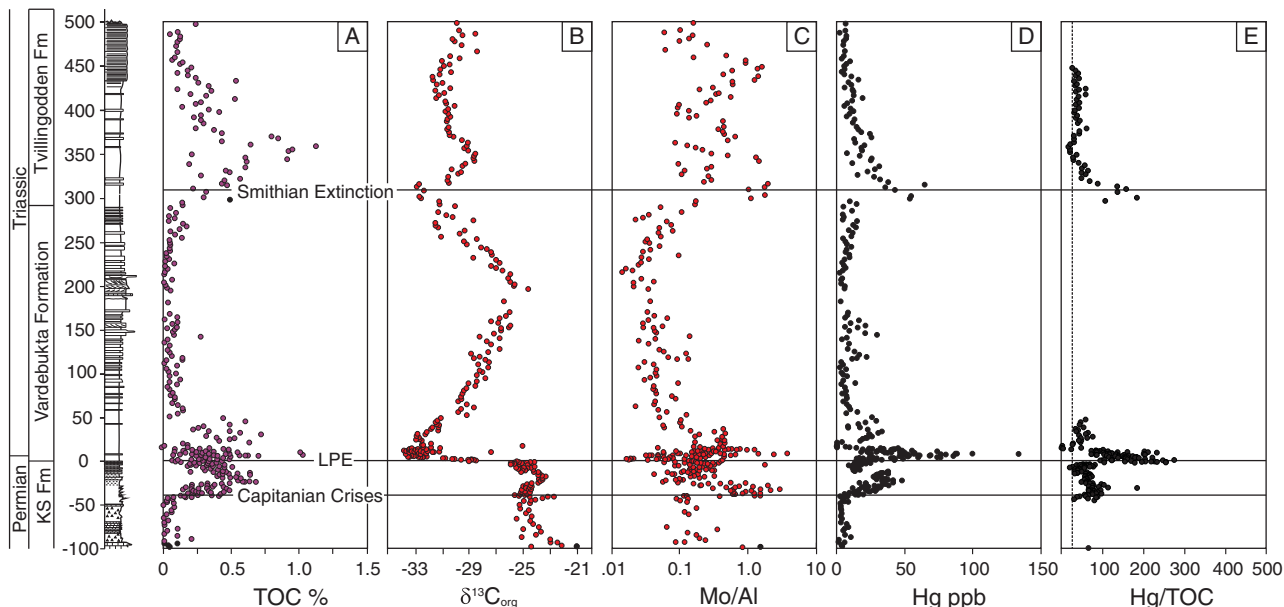
Figure 3. (Colour online) Plots of geochemical data from Festningen, showing: (a) percent total organic carbon (TOC); (b) carbon isotope values for organic carbon; (c) Mo normalized by Al; (d) Hg values; and (e) Hg normalized by TOC (the Hg/TOC values are only shown for values of TOC > 0.2 %; below that value Rock-Eval analyses provide less accurate results that are magnified in calculated ratios).

isotope record. The $\delta^{13}C_{org}$ data from Festningen show initially relatively stable values of c. −24‰ through the middle–upper Permian sediments, with a relatively minor negative shift at c. −40 m. At the top of the Kapp Starostin Formation, carbon isotope values show the onset of a pronounced 10‰ negative shift through the basal Vardebukta Formation sediments (Grasby et al. 2015). After this point there is a progressive recovery through the next 200 m, followed by another progressive negative shift to a minimum at c. +300 m which is followed by an unstable period through the remainder of the measured section (Wignall et al. this volume).

4.c. Molybdenum

Similar to the carbon isotope record, trace element data have been shown as a proxy for anoxia for the three separate portions of the section previously studied (Bond et al. 2015; Grasby et al. 2015; Wignall et al. this volume). For reference, the composite curve of Mo normalized to Al is shown through the entire interval (Fig. 3c). Results show relatively low values at the base of the section with a significant spike in Mo/Al at c. −40 m, which coincides with the shift to higher TOC values and minor negative shift in $\delta^{13}C_{org}$. Above the LPE boundary there is a second spike in Mo/Al that

initiates *c.* 5 m after the main LPE event. This is followed by a gradual decline in Mo/Al until *c.* 200 m, coincident with the reversal in the trend of carbon isotopes. The Mo/Al values progressively increase again through the next 100 m until +300 m, where peak Mo/Al ratios are coincident with the minimum in $\delta^{13}C_{org}$ values. Mo/Al values then become highly variable for the rest of the measured section.

4.d. Mercury

Hg values for the studied section, reported here for the first time, are plotted in Figure 3d. Hg values are 0.005–0.010 µg g⁻¹ in the basal 60 m of section and then show a shift above –40 m to values up to 0.050 µg g⁻¹, followed by a subsequent decline to values of *c.* 0.020 µg g⁻¹ in the 10 m just below the LPE boundary. At the LPE there is a significant spike in Hg to the highest values observed in the section (>0.130 µg g⁻¹). Hg concentrations drop rapidly to background values of 0.005–0.010 µg g⁻¹ through the remainder of the section. The only exception is a brief spike at *c.* +300 m, where Hg concentrations up to 0.065 µg g⁻¹ are observed.

In both marine and freshwater environments, dissolved Hg has been shown to have a strong affinity for organic matter (OM) (Mason, Reinfelder & Morel, 1996; Gagnon, Pelletier & Mucci, 1997; Benoit *et al.* 2001; Han *et al.* 2006; Gehrke, Blum & Meyers, 2009). Grasby *et al.* (2013*b*) have also shown that OM strongly controls Hg sequestration over geological time. Along with absolute concentrations, the Hg/TOC ratio is plotted in Figure 3e. However, TOC values are too low to be considered accurate for parts of the section, where Rock-Eval analyses cannot accurately resolve concentrations <0.2 % TOC; as a result, only samples with TOC >0.2 % are plotted as lower accuracy can greatly affect the calculated ratio. These data show a general trend where the Hg/TOC ratio has constant low values through the section. The exceptions to this are the large spikes in Hg/TOC values that occur at the LPE boundary as well as smaller shifts that occur at –40 m as well as at *c.* +300 m. These increases in Hg/TOC ratio are consistent with zones where there are large spikes in absolute Hg concentration. Hg values are low outside these three levels.

5. Discussion

5.a. Carbon isotope chemostratigraphy

The $\delta^{13}C$ record through sediments of Permian – Early Triassic age shows significant shifts that are comparable to those observed in the Sverdrup Basin (Grasby *et al.* 2013*a*) as well as with inorganic $\delta^{13}C$ trends from records in the Panthalassa (Horacek, Koike & Richoz, 2009) and the Tethys (Payne *et al.* 2004; Horacek, Brandner & Abart, 2007). This demonstrates that Festningen records global variation in biogeochemical cycles through this time interval. These can be used as

a chemostratigraphic tool to support both regional and global correlation.

Bond *et al.* (2015) argued that the minor negative carbon anomaly at –40 m correlates with the Capitanian Crisis. The LPE event, as marked by the loss of chert forming siliceous sponges, is characterized by the onset of a large negative shift in $\delta^{13}C_{org}$ that reaches a minimum in the basal Vardebukta Formation (Wignall, Morante & Newton, 1998; Grasby *et al.* 2015). Above the Kapp Starostin Formation, Wignall *et al.* (this volume) show that the next negative low point at *c.* 300 m is correlative with the end-Smithian Substage. This is also consistent with comparison to the $\delta^{13}C_{org}$ record from the Smithian stratotype (Grasby *et al.* 2013*a*), as illustrated in Figure 4. This makes the low in carbon isotope values equivalent to the Smithian/Spathian Extinction event that was associated with renewed Siberian Trap volcanism and rapid global temperature increase (Brayard *et al.* 2006; Orchard, 2007; Xie *et al.* 2010; Sun *et al.* 2012).

5.b. Mercury deposition

The Hg record at Festningen shows a relatively constant background value through the majority of the succession analysed (<0.020 µg g⁻¹). However, notable spikes in Hg concentration occur coincident with the three extinction levels represented in this section (Capitanian Crisis, LPE and Smithian/Spathian Extinction). Of these three spikes the most significant occurs at the LPE boundary. Aside from the three most prominent Hg spikes, there is also a slight increase in the upper Dienerian portion of the section. It is interesting to note that these prominent Hg spikes are all associated with shifts to lower $\delta^{13}C$ values. In addition, there is a general association of higher Hg concentrations associated with high Mo/Al values (Fig. 2). While this may suggest increased Hg sequestration associated with changes to more anoxic environments, a plot of Mo/Al versus Hg reveals that there is no correlation (Fig. 5). Despite the general relationship, the data suggest that anoxia has no direct influence on Hg sequestration in sediments.

Given the low organic matter content throughout much of the Lower Triassic portion of the studied section, reliable Hg/TOC ratios are not always possible to obtain. For values <0.2 % TOC, inaccuracies in measurement can lead to magnified errors and highly variable Hg/TOC values that are not reflective of natural conditions; these are therefore not shown here. However, for TOC values >0.2 %, the Hg/TOC ratios for the Festningen section have relatively constant background values (vertical dashed line in Fig. 3e). These results are consistent with Hg/TOC through the Lower Triassic Smithian stratotype, Sverdrup Basin (Grasby *et al.* 2013*b*), indicating a general background level of Hg sequestration into sediment that is largely controlled by organic matter deposition.

The notable exceptions to this background Hg deposition are spikes in both total Hg concentrations as well as Hg/TOC levels at the three extinction levels (Fig. 3).
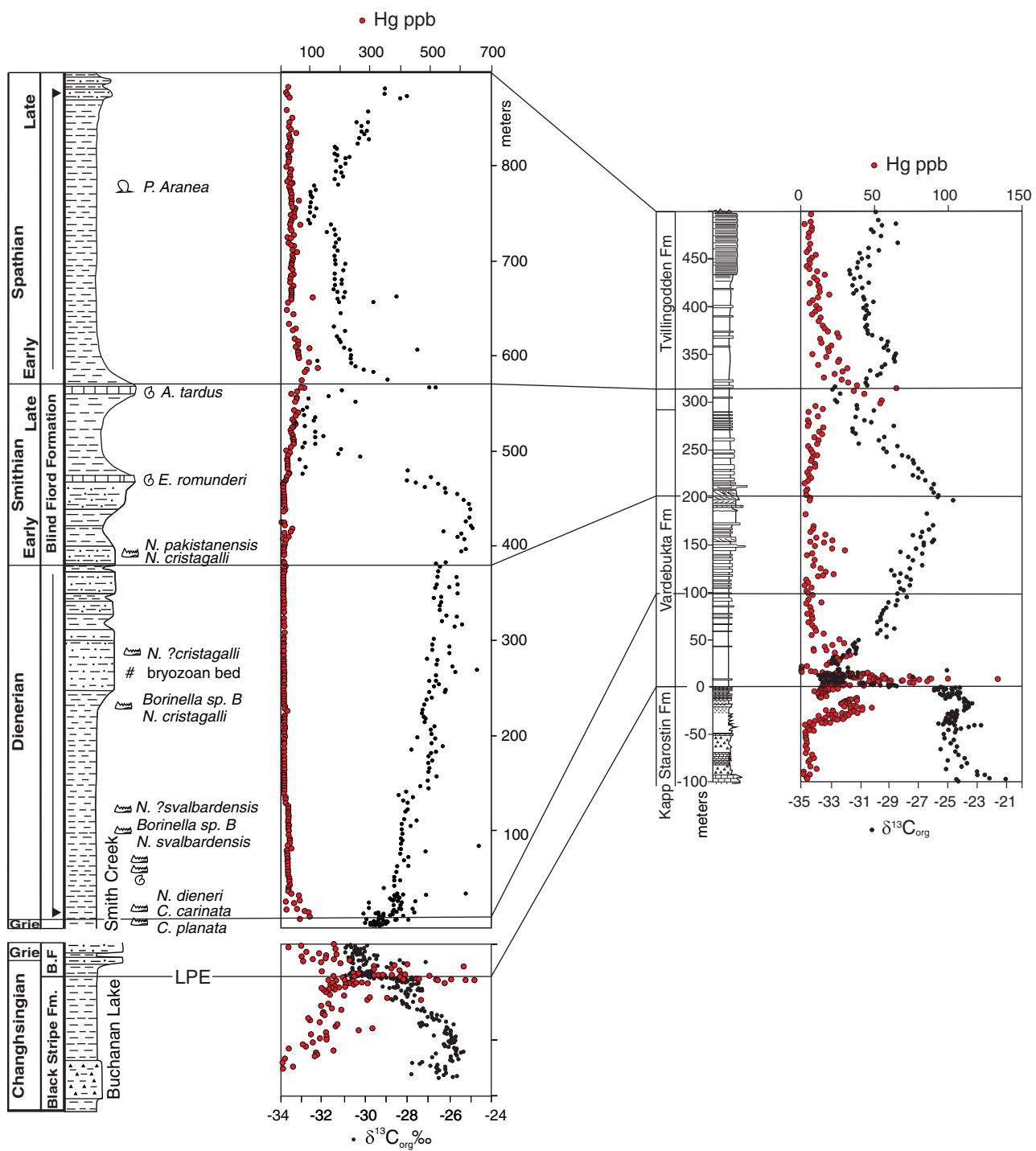
Figure 4. (Colour online) Correlation of carbon isotope and Hg records from the Smithian stratotype (left side; Grasby *et al.* 2013*a*) with record from Festningen (right side; this study).

Previously Sanei, Grasby & Beauchamp (2012) and Grasby *et al.* (2013*b*) argued that Hg anomalies in the geological record are related to massive Hg emissions associated with periods of major volcanic eruptions. Our results from Festningen provide support for this hypothesis, showing that over the *c.* 12 Ma record there are three prominent Hg anomalies superimposed on background Hg concentrations. In each case these Hg spikes are associated with global extinction events that have previously been tied to LIP eruptions: Capitanian

Crisis (Emeishan eruptions); LPE (Siberian Traps); and Smithian/Spathian Extinction (renewed Siberian Traps) (Paton *et al.* 2010; Xie *et al.* 2010; Bond & Wignall, 2014).

On a regional perspective the Hg spikes observed at Festningen closely correspond to those in the Sverdrup Basin (Fig. 4). This indicates that these periods of anomalous Hg deposition are regional in scope, and suggests periods of enhanced Hg deposition over broad areas.
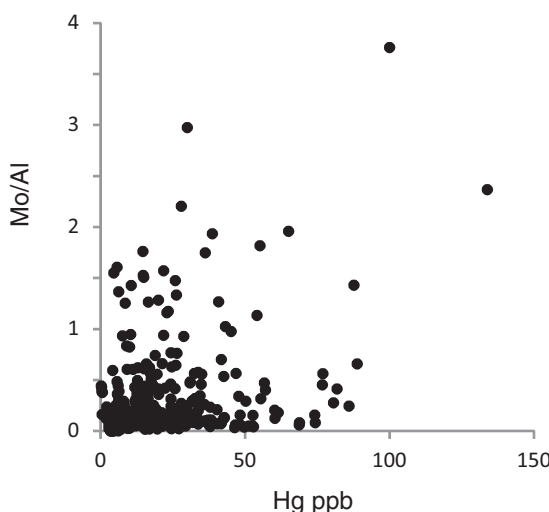
Figure 5. Plot of the Mo/Al ratio versus Hg concentration.

6. Conclusions

The organic carbon isotope records from the Festningen section show trends through sediments of late Permian – Early Triassic age that closely correspond to those of the Sverdrup Basin, as well as the global inorganic carbon record. These results illustrate that NW Pangea records perturbations to the global carbon cycle. It was previously demonstrated that Hg is an excellent proxy for periods of major volcanic activity in the geological record (Sanei, Grasby & Beauchamp, 2012; Grasby *et al.* 2013*b*; Sial *et al.* 2013). The Festningen section records a general constant background of Hg deposition through time. However, there are notable spikes in Hg concentration as well as in the Hg/TOC ratio that correspond to periods of mass extinction (Capitanian Crisis, the LPE event and the Smithian/Spathian Extinction), all of which have been associated with LIP events. Our results therefore support the use of Hg as a marker for LIP eruptions. What remains uncertain is what role such Hg release could have on ecosystems. Hg is certainly one of the most toxic elements for life, and enhanced Hg flux from large igneous events would likely have a global impact on both the terrestrial and marine realm. Our results show that there are consistent records of Hg spikes associated with LIP events and mass extinctions across NW Pangea. The global nature of these records remains to be demonstrated. If they are more widely distributed, then Hg release could have played a role as a significant extinction mechanism throughout Earth's history.

References

AMAP. 2011. *AMAP Assessment 2011: Mercury in the Arctic*. Oslo, Norway: Arctic Monitoring and Assessment Programme(AMAP).

ANDREN, A. W. & HARRISS, R. C. 1975. Observations on the association between mercury and organic matter dissolved in natural waters. *Geochimica et Cosmochimica Acta* **39**(9), 1253–58.

BEAUCHAMP, B., HENDERSON, C. M. B., GRASBY, S. E., GATES, L., BEATTY, T., UTTING, J. & JAMES, N. P. 2009. Late Permian sedimentation in the Sverdrup Basin, Canadian Arctic: the Lindström and Black Stripe formations. *Canadian Society of Petroleum Geology Bulletin* **57**, 167–91.

BENOIT, J. M., MASON, R. P., GILMOUR, C. C. & AIKEN, G. R. 2001. Constants for mercury binding by dissolved organic matter isolates from the Florida Everglades. *Geochimica et Cosmochimica Acta* **65**(24), 4445–51.

BLOMEIER, D., DUSTIRA, A. M., FORKE, H. & SCHEIBNER, C. 2013. Facies analysis and depositional environments of a storm-dominated, temperate to cold, mixed siliceous-carbonate ramp: the Permian Kapp Starostin Formation in NE Svalbard. *Norwegian Journal of Geology* **93**, 75–98.

BOND, D. P. G. & WIGNALL, P. B. 2014. Large igneous provinces and mass extinctions: An update. In *Volcanism, Impacts, and Mass Extinctions: Causes and Effects* (eds G. Keller & A. C. Kerr). Geological Society of America, Special Papers 505, doi:10.1130/2014.2505(02).

BOND, D. P. G., WIGNALL, P. B., JOACHIMSKI, M., SUN, Y., SAVOV, I., GRASBY, S. E., BEAUCHAMP, B. & BLOMEIER, D. P. G. 2015. An abrupt extinction in the Middle Permian (Capitanian) of the Boreal Realm (Spitsbergen). *Geological Society of America Bulletin*, published online 14 April 2015, doi: 10.1130/B31216.1.

BRAYARD, A., BUCHER, H., ESCARGUEL, G., FLUTEAU, F., BOURQUIN, S. & GALFETTI, T. 2006. The Early Triassic ammonoid recovery: Paleoclimatic significance of diversity gradients. *Palaeogeography, Palaeoclimatology, Palaeoecology* **239**(3–4), 374–95.

CRANSTON, R. E. & BUCKLEY, D. E. 1972. Mercury pathways in a river and estuary. *Environmental Science & Technology* **6**(3), 274–78.

EMBRY, A. 1989. Correlation of Upper Palaeozoic and Mesozoic sequences between Svalbard, Canadian Arctic Archipelago, and northern Alaska. In *Correlation in Hydrocarbon Exploration* (ed. J. D. Collinson), pp. 89–98. Netherlands: Springer.

EMBRY, A. F. 1992. Crockerland: The Northwest source area for the Sverdrup Basin, Canadian Arctic Islands. In *Arctic Geology and Petroleum Potential* (eds T. O. Vorren, E. Bergsager, Ø. A. Dahl-Stamnes, E. Holter, B. Johansen, E. Lie & T. B. Lund), pp. 205–16. Amsterdam: Elsevier.

ERWIN, D. H. 2006. *Extinction. How Life on Earth Nearly Ended 250 million years ago*. New Jersey: Princeton University Press.

GAGNON, C., PELLETIER, É. & MUCCI, A. 1997. Behaviour of anthropogenic mercury in coastal marine sediments. *Marine Chemistry* **59**(1–2), 159–76.

GEHRKE, G. E., BLUM, J. D. & MEYERS, P. A. 2009. The geochemical behavior and isotopic composition of Hg in a mid-Pleistocene western Mediterranean sapropel. *Geochimica et Cosmochimica Acta* **73**(6), 1651–65.

GOLONKA, J. & FORD, D. 2000. Pangean (Late Carboniferous–Middle Jurassic) paleoenvironment and

lithofacies. *Palaeogeography, Palaeoclimatology, Palaeoecology* **161**, 1–34.

GRASBY, S. E., BEAUCHAMP, B., BOND, D. P. G., WIGNALL, P. B., TALAVERA, C., GALLOWAY, J. M., PIEPJOHN, K., REINHARDT, L. & BLOMEIER, D. 2015. Progressive environmental deterioration in NW Pangea leading to the Latest Permian Extinction. *Geological Society of America Bulletin*, published online 14 April 2015, doi: 10.1130/B31197.1.

GRASBY, S. E., BEAUCHAMP, B., EMBRY, A. F. & SANEI, H. 2013*a*. Recurrent Early Triassic ocean anoxia. *Geology* **41**, 175–78.

GRASBY, S. E., SANEI, H., BEAUCHAMP, B. & CHEN, Z. 2013*b*. Mercury deposition through the Permo–Triassic Biotic Crisis. *Chemical Geology* **351**, 209–16.

HALL, G. & PELCHAT, P. 1997. Evaluation of a direct solid sampling atomic absorption spectrometer for the trace determination of mercury in geological samples. *Analyst* **122**(9), 921–24.

HAN, S., GILL, G. A., LEHMAN, R. D. & CHOE, K.-Y. 2006. Complexation of mercury by dissolved organic matter in surface waters of Galveston Bay, Texas. *Marine Chemistry* **98**(2–4), 156–66.

HAYES, J. M., KAPLAN, I. R. & WEDEKING, K. W. 1983. Precambrian organic geochemistry, preservation of the record. In *Earth's Earliest Biosphere: Its Origin and Evolution* (ed. J. W. Schopf), pp. 92–132. Princeton NJ: Princeton University Press.

HORACEK, M., BRANDNER, R. & ABART, R. 2007. Carbon isotope record of the P/T boundary and the Lower Triassic in the Southern Alps: Evidence for rapid changes in storage of organic carbon. *Palaeogeography, Palaeoclimatology, Palaeoecology* **252**(1–2), 347–54.

HORACEK, M., KOIKE, T. & RICHOZ, S. 2009. Lower Triassic δ^{13}C isotope curve from shallow-marine carbonates in Japan, Panthalassa realm: Confirmation of the Tethys δ^{13}C curve. *Journal of Asian Earth Sciences* **36**(6), 481–90.

KELLER, G. & KERR, A. C. (eds) 2014. *Volcanism, Impacts, and Mass Extinctions: Causes and Effects*. Boulder, CO: Geological Society of America.

LAFARGUE, E., ESPITALITÉ, J., MARQUIS, F. & PILLOT, D. 1998. Rock-Eval 6 applications in hydrocarbon exploration, production and soil contamination studies. *Revue de L'institut Francais du Petrole* **53**(4), 421–37.

LINDBERG, S. E., ANDRENSON, A. W. & HARRISSON, R. C. 1975. Geochemistry of mercury in the estuarine environment. In *Estuarine Research. Chemistry, Biology and the Estuarine System* (ed. E. L. Cronin). New York: Academic Press.

MASON, R. P., REINFELDER, J. R. & MOREL, F. M. M. 1996. Uptake, toxicity, and trophic transfer of mercury in a coastal diatom. *Environmental Science & Technology* **30**(6), 1835–45.

MØRK, A., KNARUD, R. & WORSLEY, D. 1982. Depositional and diagenetic environments of the Triassic and Lower Jurassic succession of Svalbard. In *Arctic Geology and Geophysics: Proceedings of the Third International Symposium on Arctic Geology* (eds A. F. Embry & H. R. Balkwill), pp. 371–98. Calgary: Canadian Society of Petroleum Geologists.

ORCHARD, M. J. 2007. Conodont diversity and evolution through the latest Permian and Early Triassic upheavals. *Palaeogeography, Palaeoclimatology, Palaeoecology* **252**(1–2), 93–117.

OUTRIDGE, P. M., SANEI, H., STERN, G. A., HAMILTON, P. B. & GOODARZI, F. 2007. Evidence for control of mercury accumulation in sediments by variations of aquatic primary productivity in Canadian High Arctic lakes. *Environmental Science & Technology* **41**, 5259–65.

PATON, M. T., IVANOV, A. V., FIORENTINI, M. L., MCNAUGHTON, N. J., MUDROVSKA, I., REZNITSKII, L. Z. & DEMONTEROVA, E. I. 2010. Late Permian and Early Triassic magmatic pulses in the Angara-Taseeva syncline, Southern Siberian Traps and their possible influence on the environment. *Russian Geology and Geophysics* **51**(9), 1012–20.

PAYNE, J. L., LEHRMANN, D. J., WEI, J., ORCHARD, M. J., SCHRAG, D. P. & KNOLL, A. H. 2004. Large perturbations of the carbon cycle during recovery from the End-Permian extinction. *Science* **305**, 506–9.

PIRRONE, N., CINNIRELLA, S., FENG, X., FINKELMAN, R. B., FRIEDLI, H. R., LEANER, J., MASON, R., MUKHERJEE, A. B., STRACHER, G. B., STREETS, D. G. & TELMER, K. 2010. Global mercury emissions to the atmosphere from anthropogenic and natural sources. *Atmospheric Chemistry and Physics Discussions* **10**, 4719–52.

PYLE, D. M. & MATHER, T. A. 2003. The importance of volcanic emissions for the global atmospheric mercury cycle. *Atmospheric Environment* **37**(36), 5115–24.

SANEI, H., GRASBY, S. E. & BEAUCHAMP, B. 2012. Latest Permian mercury anomalies. *Geology* **40**(1), 63–6.

SANEI, H., GRASBY, S. E. & BEAUCHAMP, B. 2015. Contaminants in marine sedimentary deposits from coal fly ash during the Latest Permian Extinction (Chapter 5). In: *Environmental Contaminants: Using Natural Archives to Track Sources and Long-Term Trends of Pollution* (J. M. Blais, M. R. Rosen & J. P. Smol, eds), pp. 89–100. Springer, Developments in Paleoenvironmental Research vol. 18.

SANEI, H., OUTRIDGE, P. M., STERN, G. A. & MACDONALD, R. W. 2014. Classification of mercury-labile organic matter relationships in lake sediments. *Chemical Geology* **373**, 87–92.

SCHUSTER, P. F., KRABBENHOFT, D. P., NAFTZ, D. L., CECIL, L. D., OLSON, M. L., DEWILD, J. F., SUSONG, D. D., GREEN, J. R. & ABBOTT, M. L. 2002. Atmospheric mercury deposition during the last 270 years: a glacial ice core record of natural and anthropogenic sources. *Environmental Science & Technology* **36**(11), 2303–10.

SCOTESE, C. R. 2004. A continental drift flipbook. *Journal of Geology* **112**, 729–41.

SIAL, A. N., CHEN, J., LACERDA, L. D., PERALTA, S., GAUCHER, C., FREI, R., CIRILLI, S., FERREIRA, V. P., MARQUILLAS, R. A., BARBOSA, J. A., PEREIRA, N. S. & BELMINO, I. K. C. 2014. High-resolution Hg chemostratigraphy: a contribution to the distinction of chemical fingerprints of the Deccan volcanism and Cretaceous–Paleogene Boundary impact event. *Palaeogeography, Palaeoclimatology, Palaeoecology* **414**, 98–115.

SIAL, A. N., LACERDA, L. D., FERREIRA, V. P., FREI, R., MARQUILLAS, R. A., BARBOSA, J. A., GAUCHER, C., WINDMÖLLER, C. C. & PEREIRA, N. S. 2013. Mercury as a proxy for volcanic activity during extreme environmental turnover: The Cretaceous–Paleogene transition. *Palaeogeography, Palaeoclimatology, Palaeoecology* **387**, 153–64.

SILVA, M. V. N., SIAL, A. N., BARBOSA, J. A., FERREIRA, V. P., NEUMANN, V. H. & DE LACERDA, L. D. 2013. Carbon isotopes, rare-earth elements and mercury geochemistry across the K–T transition of the Paraíba Basin, northeastern Brazil. In *Isotopic Studies in Cretaceous Research* (A.-V. Bojar, M. C. Melinte-Dobrinescu & J. Smit, eds), pp. 85–104. Geological Society, London, Special Publications no. 382.

SLEMR, F., JUNKERMANN, W., SCHMIDT, R. W. H. & SLADKOVIC, R. 1995. Indication of change in global and regional trends of atmospheric mercury concentrations. *Geophysical Research Letters* **22**(16), 2143–6.

SLEMR, F. & SCHEEL, H. E. 1998. Trends in atmospheric mercury concentrations at the summit of the Wank mountain, Southern Germany. *Atmospheric Environment* **32**(5), 845–53.

STEMMERIK, L. & WORSLEY, D. 2005. 30 years on: Arctic Upper Palaeozoic stratigraphy, depositional evolution and hydrocarbon prospectivity. *Norsk Geologisk Tidsskrift* **85**, 151–68.

STERN, G. A., SANEI, H., ROACH, P., DELARONDE, J. & OUTRIDGE, P. M. 2009. Historical interrelated variations of mercury and aquatic organic matter in lake sediment cores from a subarctic lake in Yukon, Canada: further evidence toward the algal-mercury scavenging hypothesis. *Environmental Science & Technology* **43**, 7684–90.

SUN, Y., JOACHIMSKI, M. M., WIGNALL, P. B., YAN, C., CHEN, Y., JIANG, H., WANG, L. & LAI, X. 2012. Lethally hot temperatures during the Early Triassic greenhouse. *Science* **338**(6105), 366–70.

TURNER, A., MILLWARD, G. E. & LE ROUX, S. M. 2004. Significance of oxides and particulate organic matter in controlling trace metal partitioning in a contaminated estuary. *Marine Chemistry* **88**(3–4), 179–92.

WIGNALL, P. B., BOND, D. P. G., SUN, Y., GRASBY, S. E., BEAUCHAMP, B., JOACHIMSKI, M. & BLOMEIER, D. This volume. Ultra-shallow marine anoxia in an Early Triassic storm-dominated clastic ramp (Spitsbergen) and the suppression of benthic radiation. *Geological Magazine*.

WIGNALL, P. B., MORANTE, R. & NEWTON, R. 1998. The Permo–Triassic transition in Spitsbergen: $\delta^{13}C_{org}$ chemostratigraphy, Fe and S geochemistry, facies, fauna and trace fossils. *Geological Magazine* **135**, 47–62.

XIE, S., PANCOST, R. D., WANG, Y., YANG, H., WIGNALL, P. B., LUO, G., JIA, C. & CHEN, L. 2010. Cyanobacterial blooms tied to volcanism during the 5 m.y. Permo–Triassic biotic crisis. *Geology* **38**(5), 447–50.